DOI:10.7511/jslx20230421001

基于薄板样条径向基函数的复合材料层合板自由振动分析

宋薇薇*[1,2,3], 项 松[1,2], 赵 锐[1,2], 赵为平[1,2], 郭 晗[1,2]

(1.沈阳航空航天大学 辽宁省通用航空重点实验室,沈阳 110136;
2.辽宁通用航空研究院,沈阳 110136; 3.沈阳航空航天大学 民用航空学院,沈阳 110136)

摘 要:基于复合材料层合板的三角剪切变形理论,推导了对称复合材料层合板的控制微分方程。利用基于薄板样条径向基函数的无网格配置方法离散的控制微分方程,预测了对称复合材料层合板的自由振动行为。计算了不同材料参数和层合板几何参数的固有频率,并与文献结果进行了比较。还研究了节点排布、模量比和边厚比对固有频率的影响。结果表明,本文结果与文献结果具有较好的一致性,节点数量越大,无量纲频率对网格分布越不敏感,固有频率随着边厚比和模量比的增加而增加。通过数值实验,证明了用薄板样条径向基函数离散的三角剪切变形理论对对称复合材料层合板的自由振动分析具有较高的数值精度和良好的收敛性。

关键词:三角剪切变形理论;复合材料层合板;自由振动;薄板样条径向基函数;固有频率
中图分类号:O342 **文献标志码**:A **文章编号**:1007-4708(2024)05-0954-09

1 引 言

近年来,复合材料由于其优越的力学性能,在航空航天、交通运输、机械和船舶工业等许多工程领域得到了广泛的应用。其具有高比强度,并具有高阻尼特性[1]。这种先进材料的另一个优点是可以提供广泛的设计方案,以满足各种工程要求。随着复合材料板的使用越来越多,迫切需要用更精确的计算理论来分析板的自由振动。

计算理论通常分为三维弹性理论、离散层理论和等效单层理论(包括经典板理论、一阶剪切变形理论和高阶剪切变形论)[2]。经典层合板理论由于忽略了横向剪切变形的影响,只能应用于薄板问题。一阶剪切变形理论虽然考虑了横向剪切变形,但是需要剪切纠正系数,剪切纠正系数的选取对计算精度有很大的影响[3]。高阶剪切变形理论(HSDT)考虑了剪切变形效应和板材上下表面的无应力边界条件,因此不需要剪切修正系数。几十年来,学者们提出了大量具有不同未知数的高阶剪切变形理论[4-9]。这些理论通常能提供令人满意的精度,但由于许多未知因素和平衡方程,通常需要较高的计算成本。一阶剪切变形理论(FSDT)一直是研究的热点。一阶剪切变形理论使用 z 的多项式来表示整个厚度上的非线性位移场。位移场的这种性质导致了不连续的横向剪切应力。Arya等[10]将三角剪切变形理论应用于复合材料层合梁。这些理论使用正弦项表示厚度上的非线性位移场。横向剪切应力和应变用余弦项表示。该模型满足界面处位移和横向剪应力的连续性。梁顶部和底部的零横向剪应力边界条件也得到满足。Ferreira等[11]还将三角剪切变形理论应用于正交铺设对称复合材料层合板的静态分析。通过比较分析三角函数剪切变形理论和三阶剪切变形理论,发现三角函数剪切变形理论更简单实用。

复合材料板的自由振动分析已有许多研究者进行过研究。Wang[12]将一阶剪切变形理论应用于角铺设纤维增强层合板的自由振动分析。Khdeir等[13]使用二阶剪切变形理论分析了角铺设和反对称角铺设复合材料层合板的自由振动行为。Khdeir等[14]使用高阶剪切变形理论分析了对称角

收稿日期:2023-04-21; **修改稿收到日期**:2023-07-22.
作者简介:宋薇薇*(1983-),女,硕士,讲师(E-mail:214097295@qq.com).
引用本文:宋薇薇,项 松,赵 锐,等.基于薄板样条径向基函数的复合材料层合板自由振动分析[J].计算力学学报,2024,**41**(5):954-962.
SONG Wei-wei, XIANG Song, ZHAO Rui, et al. Free vibration analysis of laminated composite plates based on thin plate spline radial basis functions[J]. *Chinese Journal of Computational Mechanics*, 2024, **41**(5): 954-962.

铺设弹性板的屈曲和自由振动。Akhras 等[15]将具有高阶剪切变形理论的样条有限元方法应用于复合材料层合板的静态和自由振动分析。Ferreira 等[16]通过一阶剪切变形理论和径向基函数(RBF)分析了对称角铺设复合材料板的自由振动行为。Liew 等[17]在移动最小二乘微分求积程序中采用了一阶剪切变形理论来预测中厚对称复合材料层合板的自由振动行为。

求解偏微分方程的方法包括有限元法、有限体积法或有限差分法。所有这些方法都需要一个网格来进行局部近似。近年来，Atluri 等[18-20]提出了一种无网格方法，该方法中的问题域由一组分散的节点离散化，并且不需要节点之间的单元连通性。径向基函数方法是一种无网格方法，其使用径向基函数近似偏微分方程的整体解。Kansa[21]使用径向基函数来求解偏微分方程。Ferreira 等[22-23]将复合二次径向基函数应用于分析复合材料层合板和功能梯度板。

常用的径向基函数主要有复合二次径向基函数、逆复合二次径向基函数、高斯径向基函数和薄板样条径向基函数四种。前三种径向基函数都需要复杂的过程来选择形状参数，形状参数对计算精度有较大影响。而薄板样条径向基函数不需要形状参数，大大减少了计算量。而对于移动最小二乘法，对其进行拟合时，其权函数随着节点不停移动，也造成了移动最小二乘法的计算量相对较大。

因此，本文利用薄板样条径向基函数[10]和三角剪切变形理论对复合材料层合板的自由振动进行分析。通过算例研究不同网格分布、模量比和边厚比对固有频率的影响以及收敛特性。将本文结果与文献结果进行了比较，两者具有较好的一致性。数值算例证明，采用薄板样条径向基函数对复合材料层合板进行自由振动分析，具有较高的精度和良好的收敛性。

2　基于三角剪切变形理论的微分控制方程

基于三角剪切变形理论，具有全局厚度 h 的对称复合材料层合板的位移场可以定义为

$$\begin{aligned} u &= -z(\partial w(x,y)/\partial x) + [\sin(\pi z/h)]\Phi_x(x,y) \\ v &= -z(\partial w(x,y)/\partial y) + [\sin(\pi z/h)]\Phi_y(x,y) \\ w &= w(x,y) \end{aligned} \tag{1}$$

式中 w 是挠度，Φ_x 和 Φ_y 分别是中间平面法线绕 y 轴和 x 轴的旋转。应变-位移关系为

$$\begin{Bmatrix} \varepsilon_{xx} \\ \varepsilon_{yy} \\ \gamma_{xy} \\ \gamma_{yz} \\ \gamma_{xz} \end{Bmatrix} = \begin{Bmatrix} \partial u/\partial x \\ \partial v/\partial y \\ \partial u/\partial y + \partial v/\partial x \\ \partial v/\partial z + \partial w/\partial y \\ \partial u/\partial z + \partial w/\partial x \end{Bmatrix} \tag{2}$$

通过将式(1)代入式(2)，应变可表示为

$$\begin{Bmatrix} \varepsilon_{xx} \\ \varepsilon_{yy} \\ \gamma_{xy} \end{Bmatrix} = z\begin{Bmatrix} -\partial^2 w/\partial x^2 \\ -\partial^2 w/\partial y^2 \\ -2\dfrac{\partial^2 w}{\partial x\,\partial y} \end{Bmatrix} + \sin\frac{\pi z}{h}\begin{Bmatrix} \partial\Phi_x/\partial x \\ \partial\Phi_y/\partial y \\ \dfrac{\partial\Phi_x}{\partial y} + \dfrac{\partial\Phi_y}{\partial x} \end{Bmatrix} \tag{3}$$

$$\begin{Bmatrix} \gamma_{yz} \\ \gamma_{xz} \end{Bmatrix} = \frac{\pi}{h}\cos\frac{\pi z}{h}\begin{Bmatrix} \Phi_y \\ \Phi_x \end{Bmatrix} \tag{4}$$

全局 x-y-z 坐标系中的应力-应变关系可表示为

$$\begin{Bmatrix} \sigma_{xx} \\ \sigma_{yy} \\ \tau_{xy} \\ \tau_{yz} \\ \tau_{zx} \end{Bmatrix} = \begin{bmatrix} \bar{Q}_{11} & \bar{Q}_{12} & \bar{Q}_{16} & 0 & 0 \\ \bar{Q}_{12} & \bar{Q}_{22} & \bar{Q}_{26} & 0 & 0 \\ \bar{Q}_{16} & \bar{Q}_{26} & \bar{Q}_{66} & 0 & 0 \\ 0 & 0 & 0 & \bar{Q}_{44} & \bar{Q}_{45} \\ 0 & 0 & 0 & \bar{Q}_{45} & \bar{Q}_{55} \end{bmatrix} \begin{Bmatrix} \varepsilon_{xx} \\ \varepsilon_{yy} \\ \gamma_{xy} \\ \gamma_{yz} \\ \gamma_{zx} \end{Bmatrix} \tag{5}$$

式中

$$\begin{aligned} \bar{Q}_{11} &= Q_{11}\cos^4\theta + 2(Q_{12}+2Q_{66})\sin^2\theta\cos^2\theta + Q_{22}\sin^4\theta \\ \bar{Q}_{12} &= (Q_{11}+Q_{22}-4Q_{66})\sin^2\theta\cos^2\theta + Q_{12}(\sin^4\theta+\cos^4\theta) \\ \bar{Q}_{16} &= (Q_{11}-Q_{12}-2Q_{66})\sin\theta\cos^3\theta + (Q_{12}-Q_{22}+2Q_{66})\sin^3\theta\cos\theta \\ \bar{Q}_{22} &= Q_{11}\sin^4\theta + 2(Q_{12}+2Q_{66})\sin^2\theta\cos^2\theta + Q_{22}\cos^4\theta \\ \bar{Q}_{26} &= (Q_{11}-Q_{12}-2Q_{66})\sin^3\theta\cos\theta + (Q_{12}-Q_{22}+2Q_{66})\sin\theta\cos^3\theta \\ \bar{Q}_{66} &= (Q_{11}+Q_{22}-2Q_{12}-2Q_{66})\sin^2\theta\cos^2\theta + Q_{66}(\sin^4\theta+\cos^4\theta) \\ \bar{Q}_{44} &= Q_{44}\cos^2\theta + Q_{55}\sin^2\theta \\ \bar{Q}_{45} &= (Q_{55}-Q_{44})\cos\theta\sin\theta \\ \bar{Q}_{55} &= Q_{55}\cos^2\theta + Q_{44}\sin^2\theta \end{aligned} \tag{6}$$

式中 θ 为 1 轴和 x 轴之间的角度，1 轴是第一主材料轴，降低刚度的分量为

$$\begin{aligned} &Q_{11} = \frac{E_1}{1-v_{12}v_{21}},\ Q_{22} = \frac{E_2}{1-v_{12}v_{21}},\ Q_{12} = v_{21}Q_{11} \\ &Q_{66} = G_{12},\ Q_{44} = G_{23},\ Q_{55} = G_{13},\ v_{21}E_1 = v_{12}E_2 \end{aligned} \tag{7}$$

式中 E_{ij}，v_{ij} 和 G_{ij} 分别为杨氏模量、泊松比和剪切模量。

利用虚功原理导出的欧拉-拉格朗日方程为

$$\begin{aligned} &\frac{\partial^2 M_{xx}}{\partial x^2} + \frac{\partial^2 M_{yy}}{\partial y^2} + 2\frac{\partial^2 M_{xy}}{\partial x\,\partial y} = I_1\frac{\partial^2 w}{\partial t^2} \\ &\frac{\partial N_{xx}}{\partial x} + \frac{\partial N_{xy}}{\partial y} - \frac{\pi}{h}Tc_{xz} = I_2\frac{\partial^2\phi_x}{\partial t^2} \\ &\frac{\partial N_{yy}}{\partial y} + \frac{\partial N_{xy}}{\partial x} - \frac{\pi}{h}Tc_{yz} = I_2\frac{\partial^2\phi_y}{\partial t^2} \end{aligned} \tag{8}$$

式中

$$\begin{Bmatrix} N_{\alpha\beta} \\ M_{\alpha\beta} \end{Bmatrix} = \int_{-h/2}^{h/2} \sigma_{\alpha\beta} \begin{Bmatrix} \sin\pi z/h \\ z \end{Bmatrix} \mathrm{d}z \tag{9}$$

$$Tc_{\alpha z} = \int_{-h/2}^{h/2} \sigma_{\alpha z} \cos(\pi z/h)\,\mathrm{d}z \tag{10}$$

式中 α 和 β 为符号 x 和 y，质量惯性 I_i 可定义为

$$I_1 = \int_{-h/2}^{h/2} \rho\,\mathrm{d}z,\ I_2 = \int_{-h/2}^{h/2} \rho z^2\,\mathrm{d}z$$

式中 ρ 为材料密度。

微分控制方程可以通过将式(9,10)代入式(8)获得

$$\begin{aligned} & zs_{11}\frac{\partial^3\Phi_x}{\partial x^3} + (zs_{12}+2zs_{66})\frac{\partial^3\Phi_x}{\partial x\partial y^2} + \\ & (zs_{16}+2zz_{16})\frac{\partial^3\Phi_x}{\partial x^2\partial y} + zs_{26}\frac{\partial^3\Phi_x}{\partial y^3} + \\ & (zs_{12}+2zs_{66})\frac{\partial^3\Phi_y}{\partial x^2\partial y} + zs_{22}\frac{\partial^3\Phi_y}{\partial y^3} + \\ & zs_{16}\frac{\partial^3\Phi_y}{\partial x^3} + 3zs_{26}\frac{\partial^3\Phi_y}{\partial x\partial y^2} - zz_{11}\frac{\partial^4 w}{\partial x^4} - \\ & zz_{22}\frac{\partial^4 w}{\partial y^4} - 2zz_{12}\frac{\partial^4 w}{\partial x^2\partial y^2} - 4zz_{66}\frac{\partial^4 w}{\partial x^2\partial y^2} - \\ & 4zz_{16}\frac{\partial^4 w}{\partial x^3\partial y} - 4zz_{26}\frac{\partial^4 w}{\partial x\partial y^3} = I_1\frac{\partial^2 w}{\partial t^2} \end{aligned} \tag{11}$$

$$\begin{aligned} & ss_{11}\frac{\partial^2\Phi_x}{\partial x^2} + ss_{66}\frac{\partial^2\Phi_x}{\partial y^2} - cc_{55}\left(\frac{\pi}{h}\right)^2\Phi_x + 2ss_{16}\frac{\partial^2\Phi_x}{\partial x\partial y} + \\ & ss_{16}\frac{\partial^2\Phi_y}{\partial x^2} + (ss_{12}+ss_{66})\frac{\partial^2\Phi_y}{\partial x\partial y} + ss_{26}\frac{\partial^2\Phi_y}{\partial y^2} - \\ & cc_{45}\left(\frac{\pi}{h}\right)^2\Phi_y - zs_{11}\frac{\partial^3 w}{\partial x^3} - (zs_{12}+2zs_{66})\frac{\partial^3 w}{\partial x\partial y^2} - \\ & 2zs_{16}\frac{\partial^2 w}{\partial x\partial y} - zs_{16}\frac{\partial^3 w}{\partial x^2\partial y} - zs_{26}\frac{\partial^3 w}{\partial y^3} = I_2\frac{\partial^2\Phi_x}{\partial t^2} \end{aligned} \tag{12}$$

$$\begin{aligned} & ss_{12}\frac{\partial^2\Phi_x}{\partial x\partial y} + ss_{66}\frac{\partial^2\Phi_x}{\partial x\partial y} + ss_{26}\frac{\partial^2\Phi_x}{\partial y^2} + ss_{16}\frac{\partial^2\Phi_x}{\partial x^2} - \\ & cc_{45}\left(\frac{\pi}{h}\right)^2\Phi_x + ss_{22}\frac{\partial^2\Phi_y}{\partial y^2} + ss_{66}\frac{\partial^2\Phi_y}{\partial x^2} - cc_{44}\left(\frac{\pi}{h}\right)^2\Phi_y + \\ & 2ss_{26}\frac{\partial^2\Phi_y}{\partial x\partial y} - zs_{22}\frac{\partial^3 w}{\partial y^3} - (zs_{12}+2zs_{66})\frac{\partial^3 w}{\partial x^2\partial y} - \\ & 3zs_{26}\frac{\partial^3 w}{\partial x\partial y^2} - zs_{16}\frac{\partial^3 w}{\partial x^3} = I_2\frac{\partial^2\Phi_y}{\partial t^2} \end{aligned} \tag{13}$$

式中 ss_{ij}，zs_{ij}，zz_{ij} 和 cc_{ij} 分别为弯曲刚度和剪切刚度分量，定义为

$$ss_{ij} = \sum_{k=1}^{n} \bar{Q}_{ij}^{(k)} \int_{z_k}^{z_{k+1}} \sin^2\left(\frac{\pi z}{h}\right)\mathrm{d}z \tag{14}$$

$$zs_{ij} = \sum_{k=1}^{n} \bar{Q}_{ij}^{(k)} \int_{z_k}^{z_{k+1}} z\sin\left(\frac{\pi z}{h}\right)\mathrm{d}z \tag{15}$$

$$zz_{ij} = \sum_{k=1}^{n} \bar{Q}_{ij}^{(k)} \int_{z_k}^{z_{k+1}} z^2\,\mathrm{d}z \qquad (i,j=1,2,6) \tag{16}$$

$$cc_{ij} = \sum_{k=1}^{n} \bar{Q}_{ij}^{(k)} \int_{z_k}^{z_{k+1}} \cos^2\left(\frac{\pi z}{h}\right)\mathrm{d}z\ (i,j=4,5) \tag{17}$$

式中 n 为层的总数，z_k 和 z_{k+1} 为第 k 层的下 z 坐标和上 z 坐标。

具有简支和固支的任意边缘的边界条件如下。

简支 $x=0,\ a:\ w=0,\ \Phi_y=0,\ M_x=0$

$$y=0,\ b:\ w=0,\ \Phi_x=0,\ M_y=0 \tag{18}$$

固支 $$w=0,\ \Phi_x=\Phi_y=0 \tag{19}$$

式中

$$M_x = zs_{11}\frac{\partial\Phi_x}{\partial x} + zs_{16}\frac{\partial\Phi_x}{\partial y} + zs_{12}\frac{\partial\Phi_y}{\partial y} + zs_{16}\frac{\partial\Phi_y}{\partial x} - zz_{11}\frac{\partial^2 w}{\partial x^2} - zz_{12}\frac{\partial^2 w}{\partial y^2} - 2zz_{16}\frac{\partial^2 w}{\partial x\partial y} \tag{20}$$

$$M_y = zs_{12}\frac{\partial\Phi_x}{\partial x} + zs_{26}\frac{\partial\Phi_x}{\partial y} + zs_{22}\frac{\partial\Phi_y}{\partial y} + zs_{26}\frac{\partial\Phi_y}{\partial x} - zz_{12}\frac{\partial^2 w}{\partial x^2} - zz_{22}\frac{\partial^2 w}{\partial y^2} - 2zz_{26}\frac{\partial^2 w}{\partial x\partial y} \tag{21}$$

假设 w,Φ_x 和 Φ_y 的解可以用以下形式表示

$$\begin{aligned} w &= W(x,y)\,e^{i\omega t} \\ \Phi_x &= \phi_x(x,y)\,e^{i\omega t} \\ \Phi_y &= \phi_y(x,y)\,e^{i\omega t} \end{aligned} \tag{22}$$

式中 ω 为自由振动的固有频率。将式(22)代入式(11～13)，可以根据 W，ϕ_x 和 ϕ_y 得出以下方程

$$\begin{aligned} & zs_{11}\frac{\partial^3\phi_x}{\partial x^3} + (zs_{12}+2zs_{66})\frac{\partial^3\phi_x}{\partial x\partial y^2} + (zs_{16}+2zz_{16})\times \\ & \frac{\partial^3\phi_x}{\partial x^2\partial y} + zs_{26}\frac{\partial^3\phi_x}{\partial y^3} + (zs_{12}+2zs_{66})\frac{\partial^3\phi_y}{\partial x^2\partial y} + \\ & zs_{22}\frac{\partial^3\phi_y}{\partial y^3} + zs_{16}\frac{\partial^3\phi_y}{\partial x^3} + 3zs_{26}\frac{\partial^3\phi_y}{\partial x\partial y^2} - zz_{11}\frac{\partial^4 W}{\partial x^4} - \\ & zz_{22}\frac{\partial^4 W}{\partial y^4} - 2zz_{12}\frac{\partial^4 W}{\partial x^2\partial y^2} - 4zz_{66}\frac{\partial^4 W}{\partial x^2\partial y^2} - \\ & 4zz_{16}\frac{\partial^4 W}{\partial x^3\partial y} - 4zz_{26}\frac{\partial^4 W}{\partial x\partial y^3} = -I_1\omega^2 W \end{aligned} \tag{23}$$

$$\begin{aligned} & ss_{11}\frac{\partial^2\phi_x}{\partial x^2} + ss_{66}\frac{\partial^2\phi_x}{\partial y^2} - cc_{55}\left(\frac{\pi}{h}\right)^2\phi_x + 2ss_{16}\frac{\partial^2\phi_x}{\partial x\partial y} + \\ & ss_{16}\frac{\partial^2\phi_y}{\partial x^2} + (ss_{12}+ss_{66})\frac{\partial^2\phi_y}{\partial x\partial y} + ss_{26}\frac{\partial^2\phi_y}{\partial y^2} - \\ & cc_{45}\left(\frac{\pi}{h}\right)^2\phi_y - zs_{11}\frac{\partial^3 W}{\partial x^3} - (zs_{12}+2zs_{66})\frac{\partial^3 W}{\partial x\partial y^2} - \\ & 2zs_{16}\frac{\partial^2 W}{\partial x\partial y} - zs_{16}\frac{\partial^3 W}{\partial x^2\partial y} - zs_{26}\frac{\partial^3 W}{\partial y^3} = -I_2\omega^2\phi_x \end{aligned} \tag{24}$$

$$\begin{aligned} & ss_{12}\frac{\partial^2\phi_x}{\partial x\partial y} + ss_{66}\frac{\partial^2\phi_x}{\partial x\partial y} + ss_{26}\frac{\partial^2\phi_x}{\partial y^2} + ss_{16}\frac{\partial^2\phi_x}{\partial x^2} - \\ & cc_{45}\left(\frac{\pi}{h}\right)^2\phi_x + ss_{22}\frac{\partial^2\phi_y}{\partial y^2} + ss_{66}\frac{\partial^2\phi_y}{\partial x^2} - cc_{44}\left(\frac{\pi}{h}\right)^2\phi_y + \\ & 2ss_{26}\frac{\partial^2\phi_y}{\partial x\partial y} - zs_{22}\frac{\partial^3 W}{\partial y^3} - (zs_{12}+2zs_{66})\frac{\partial^3 W}{\partial x^2\partial y} - \\ & 3zs_{26}\frac{\partial^3 W}{\partial x\partial y^2} - zs_{16}\frac{\partial^3 W}{\partial x^3} = -I_2\omega^2\phi_y \end{aligned} \tag{25}$$

3　径向基函数法

方程式(23～25)和边界条件可表示为

$$Lu(X)=\lambda u(X)\quad(X\in\Omega)$$
$$Bu(X)=0\quad(X\in\partial\Omega)\tag{26}$$

式中 $\partial\Omega$ 为区域 Ω 的边界，L 为线性椭圆偏微分算子，B 为线性边界算子，λ 为常数。方程(26)的解可以近似表达为

$$u^h(X)=\sum_{j=1}^{N}\alpha_j g(r_{ij})e^{i\omega t}\tag{27}$$

式中 N 为节点总数，α_j 为未知系数，ω 为自由振动的固有频率，$g(r_{ij})$ 为径向基函数，r_{ij} 为节点 X_i 和节点 X_j 的距离，复合二次曲面径向基函数、逆复合二次曲线径向基函数、高斯径向基函数和薄板样条径向基函数都包含一个对计算精度有重要影响的形状参数。薄板样条径向基函数中形状参数的选择比其他径向基函数更容易。本文使用的径向基函数是薄板样条径向基函数，经过大量的计算研究，当形状参数 $m=4$ 时，径向基函数计算精度最高。径向基函数为

$$g=r_{ij}^{2m}\log_{10}^{r_{ij}}\tag{28}$$

当两个节点之间的距离为零时，薄板样条径向基函数具有奇异性的缺点。为了消除薄板样条径向基函数的奇异性，当两个节点之间的距离为零时，$r_{ij}^2=r_{ij}^2+\zeta$，其中 ζ 为无穷小。本文的无穷小数值是 1×10^{-60}。

假设在区域 Ω 的内部有 N_1 个节点，在边界 $\partial\Omega$ 上有 N_B 个节点。

对于内部节点，有

$$\sum_{j=1}^{N}\alpha_j L\,g(r_{ij})=\lambda\sum_{j=1}^{N}\alpha_j g(r_{ij})\quad(i=1,\cdots,N_1)\tag{29}$$

对于边界节点，有

$$\sum_{j=1}^{N}\alpha_j B\,g(r_{ij})=0\quad(i=N_1+1,\cdots,N)\tag{30}$$

方程式(29)和(30)可以表示为

$$\begin{bmatrix}Lg\\Bg\end{bmatrix}\{\alpha\}=\lambda\begin{bmatrix}g\\0\end{bmatrix}\{\alpha\}\tag{31}$$

然后

$$\begin{bmatrix}Lg\\Bg\end{bmatrix}^{-1}\begin{bmatrix}g\\0\end{bmatrix}\alpha=\frac{1}{\lambda}\alpha\tag{32}$$

式中 $1/\lambda$ 为特征值，α 为特征向量，可以通过标准代码来求解。

根据径向基函数无网格配置方法，W，Φ_x 和 Φ_y 及其导数可离散为

$$W=\sum_{j=1}^{N}\alpha_j^W g_j,\ \Phi_x=\sum_{j=1}^{N}\alpha_j^{\Phi_x}g_j\tag{33,34}$$

$$\Phi_y=\sum_{j=1}^{N}\alpha_j^{\Phi_y}g_j,\ \frac{\partial^2 W}{\partial x^2}=\sum_{j=1}^{N}\alpha_j^W\frac{\partial^2 g_j}{\partial x^2}\tag{35,36}$$

$$\frac{\partial^2\Phi_x}{\partial y^2}=\sum_{j=1}^{N}\alpha_j^{\Phi_x}\frac{\partial^2 g_j}{\partial y^2}\tag{37}$$

将离散的 W，Φ_x 和 Φ_y 及其导数代入微分控制方程，得

$$\sum_{j=1}^{N}\alpha_j^{\Phi_x}\Big[zs_{11}\frac{\partial^3 g_j}{\partial x^3}+(zs_{12}+2zs_{66})\frac{\partial^3 g_j}{\partial x\partial y^2}+(zs_{16}+2zz_{16})\frac{\partial^3 g_j}{\partial x^2\partial y}+zs_{26}\frac{\partial^3 g_j}{\partial y^3}\Big]+\sum_{j=1}^{N}\alpha_j^{\Phi_y}\Big[zs_{16}\frac{\partial^3 g_j}{\partial x^3}+(zs_{12}+2zs_{66})\frac{\partial^3 g_j}{\partial x^2\partial y}+3zs_{26}\frac{\partial^3 g_j}{\partial x\partial y^2}+zs_{22}\frac{\partial^3 g_j}{\partial y^3}\Big]+\sum_{j=1}^{N}\alpha_j^{W}\Big[-zz_{11}\frac{\partial^4 g_j}{\partial x^4}-zz_{22}\frac{\partial^4 g_j}{\partial y^4}-2zz_{12}\frac{\partial^4 g_j}{\partial x^2\partial y^2}-4zz_{66}\frac{\partial^4 g_j}{\partial x^2\partial y^2}-4zz_{16}\frac{\partial^4 g_j}{\partial x^3\partial y}-4zz_{26}\frac{\partial^4 g_j}{\partial x\partial y^3}\Big]=-I_1\omega^2\sum_{j=1}^{N}\alpha_j^W g_j\tag{38}$$

$$\sum_{j=1}^{N}\alpha_j^{\Phi_x}\Big[ss_{11}\frac{\partial^2 g_j}{\partial x^2}+ss_{66}\frac{\partial^2 g_j}{\partial y^2}-cc_{55}\Big(\frac{\pi}{h}\Big)^2 g_j+2ss_{16}\times\frac{\partial^2 g_j}{\partial x\partial y}\Big]+\sum_{j=1}^{N}\alpha_j^{\Phi_y}\Big[ss_{16}\frac{\partial^2 g_j}{\partial x^2}+(ss_{12}+ss_{66})\frac{\partial^2 g_j}{\partial x\partial y}+ss_{26}\frac{\partial^2 g_j}{\partial y^2}-cc_{45}\Big(\frac{\pi}{h}\Big)^2 g_j\Big]+\sum_{j=1}^{N}\alpha_j^{W}\Big[-zs_{11}\frac{\partial^3 g_j}{\partial x^3}-(zs_{12}+2zs_{66})\frac{\partial^3 g_j}{\partial x\partial y^2}-2zs_{16}\frac{\partial^3 g_j}{\partial x\partial y}-zs_{16}\frac{\partial^3 g_j}{\partial x^2\partial y}-zs_{26}\frac{\partial^3 g_j}{\partial y^3}\Big]=-I_2\omega^2\sum_{j=1}^{N}\alpha_j^{\Phi_x}g_j\tag{39}$$

$$\sum_{j=1}^{N}\alpha_j^{\Phi_x}\Big[ss_{12}\frac{\partial^2 g_j}{\partial x\partial y}+ss_{66}\frac{\partial^2 g_j}{\partial x\partial y}+ss_{26}\frac{\partial^2 g_j}{\partial y^2}+ss_{16}\frac{\partial^2 g_j}{\partial x^2}-cc_{45}\Big(\frac{\pi}{h}\Big)^2 g_j\Big]+\sum_{j=1}^{N}\alpha_j^{\Phi_y}\Big[ss_{22}\frac{\partial^2 g_j}{\partial y^2}+ss_{66}\frac{\partial^2 g_j}{\partial x^2}+2ss_{26}\frac{\partial^2 g_j}{\partial x\partial y}-cc_{44}\Big(\frac{\pi}{h}\Big)^2 g_j\Big]+\sum_{j=1}^{N}\alpha_j^{W}\Big[-zs_{22}\frac{\partial^3 g_j}{\partial y^3}-(zs_{12}+2zs_{66})\frac{\partial^3 g_j}{\partial x^2\partial y}-3zs_{26}\frac{\partial^3 g_j}{\partial x\partial y^2}-zs_{16}\frac{\partial^3 g_j}{\partial x^3}\Big]=-I_2\omega^2\sum_{j=1}^{N}\alpha_j^{\Phi_y}g_j\tag{40}$$

$x=0$ 处的简支边界条件，α 边可离散为

$$W=\sum_{j=1}^{N}\alpha_j^W g_j=0,\ \Phi_y=\sum_{j=1}^{N}\alpha_j^{\Phi_y}g_j=0\tag{41,42}$$

$$M_x=\sum_{j=1}^{N}\alpha_j^{\Phi_x}\Big[zs_{11}\frac{\partial g_j}{\partial x}+zs_{16}\frac{\partial g_j}{\partial y}\Big]+\sum_{j=1}^{N}\alpha_j^{\Phi_y}\Big[zs_{16}\frac{\partial g_j}{\partial x}+zs_{12}\frac{\partial g_j}{\partial y}\Big]+\sum_{j=1}^{N}\alpha_j^{W}\Big[-zz_{11}\frac{\partial^2 g_j}{\partial x^2}-2zz_{16}\frac{\partial^2 g_j}{\partial x\partial y}-zz_{12}\frac{\partial^2 g_j}{\partial y^2}\Big]=0\tag{43}$$

式(38～43)可用式(32)的形式表示,其中 $\lambda=\omega^2$,式(32)的特征值 $1/\lambda$ 可通过标准特征值求解器求解,则 $\omega=\sqrt{\lambda}$。

4 数值示例

假设采用的层合板的所有层都具有相同的厚度,并且由相同的材料制成。每层的材料特性如下

$$E_1/E_2=10,20,30,40$$

$$G_{12}=G_{13}=0.6E_2$$

$$G_{23}=0.5E_2,\ \upsilon_{12}=0.25,\ \rho=1$$

方程(28)是本文使用的径向基函数。无量纲固有频率可以通过式(44)获得

$$\bar{\omega}=(\omega a^2/h)\sqrt{\rho/E_2} \tag{44}$$

4.1 收敛性研究

使用边 a 和厚度 h,同时 $E_1/E_2=40$,$a/h=10$ 的简支方形板(0°/90°/0°)来检查本文公式的收敛性。自然频率通过方程(44)进行了无量纲化。该板通过规则节点排布离散化(图 1),图 2 和图 3 显示了随着网格分布从 9×9 增加到 21×21,无量纲频率收敛到 Khdeir[14]的精确值。

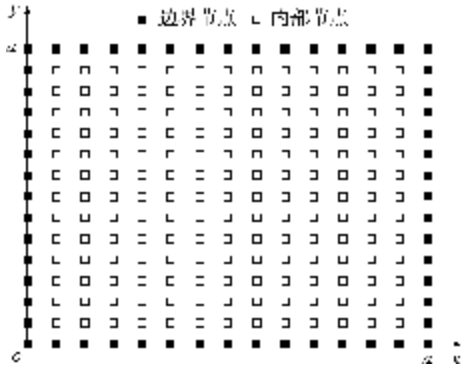

图 1 方形板 15×15 节点离散

Fig. 1 15×15 nodal distribution of square laminated plate

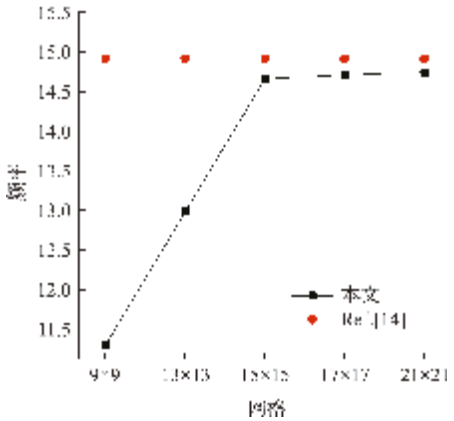

图 2 简支方形板(0°/90°/0°)一阶固有频率的收敛性研究 ($E_1/E_2=40$, $a/h=10$)

Fig. 2 Convergence study of first-order natural frequency for simply supported square plates (0°/90°/0°) ($E_1/E_2=40$, $a/h=10$)

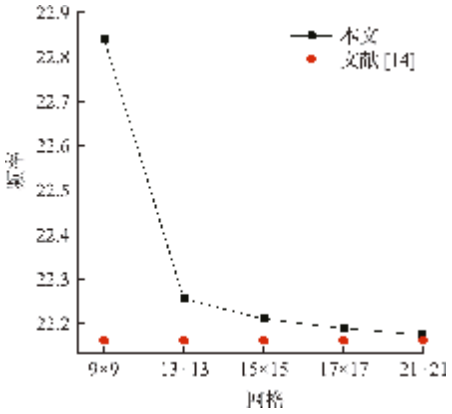

图 3 简支方形板(0°/90°/0°)二阶固有频率的收敛性研究 ($E_1/E_2=40$, $a/h=10$)

Fig. 3 Convergence study of second-order natural frequency for simply supported square plates (0°/90°/0°) ($E_1/E_2=40$, $a/h=10$)

4.2 比较研究

为了验证基于薄板样条径向基函数的数值精度,本文进行了比较研究。研究中使用 21×21 的规则节点排布。首先,考虑正交层合板的简支方形板(0°/90°/90°/0°)。不同模量比 E_1/E_2 和边厚比 a/h 的简支层合板的无量纲基频列入表 1。

表 1 四边简支四层板无量纲一阶固有频率

Tab. 1 Non-dimensional fundamental frequency of the simply supported square laminated plate

边厚比(a/h)	方法	模量比(E_1/E_2)			
		10	20	30	40
5	Ref.[24]	8.272	9.526	10.272	10.787
	Ref.[25]	8.080	9.440	10.238	10.789
	本文(21×21)	8.3932	9.6221	10.3367	10.8376
10	Ref.[24]	9.853	12.383	13.892	15.143
	Ref.[25]	9.670	12.115	13.799	15.068
	本文(21×21)	9.8999	12.2794	13.9246	15.1588

表 1 列出了四边简支四层板(0°/90°/90°/0°),当 a/h 和 E_1/E_2 取不同值时,无量纲第一阶固有频率的计算结果,并与文献[24,25]的结果进行对比。可以看出,本文计算结果与文献[24,25]的结果具有较好的一致性,固有频率随着 a/h 和 E_1/E_2 的增加而增加。

表 2 列出了四边简支四层板(0°/90°/90°/0°),当 $E_1/E_2=40$,a/h 取不同值时,无量纲第一阶固有频率的计算结果。结果表明,本文方法计算无量纲一阶固有频率的结果与文献[26,27]的结果具有一致性。

此处考虑三层方形层合板(0°/90°/0°)。表 3 列出了模量比为 $E_1/E_2=40$ 和各种边厚比 a/h 的

简支层合板的无量纲基频。研究发现，本文结果与Reddy[24]的值一致。

表2　四边简支四层板无量纲一阶固有频率（$E_1/E_2=40$）

Tab. 2　Non-dimensional fundamental frequency of the simply supported square laminated plate ($E_1/E_2=40$)

边厚比(a/h)	方法	$\bar{\omega}$
4	Ref.[26]	9.497
	Ref.[27]	9.322
	本文(21×21)	9.3447
10	Ref.[26]	15.270
	Ref.[27]	15.103
	本文(21×21)	15.1588
20	Ref.[26]	17.668
	Ref.[27]	17.641
	本文(21×21)	17.6698

表3　简支方形板（0°/90°/0°）（$E_1/E_2=40$）的无量纲一阶固有频率

Tab. 3　Non-dimensional fundamental frequency of the simply supported square plate (0°/90°/0°) ($E_1/E_2=40$)

边厚比(a/h)	方法	$\bar{\omega}$
2	Ref.[24]	5.205
	本文(21×21)	5.0905
5	Ref.[24]	10.290
	本文(21×21)	10.3307
10	Ref.[24]	14.767
	本文(21×21)	14.7449
100	Ref.[24]	18.891
	本文(21×21)	18.8278

表4列出了四边简支三层板（0°/90°/0°），当$E_1/E_2=40$，a/h取不同值时，无量纲第一阶固有频率的计算结果。结果表明，本文方法计算无量纲一阶固有频率的结果与文献[26,27]的结果具有较好的一致性。

4.3　网格分布、模量比和边厚比对固有频率的影响

考虑三层板（0°/90°/0°）和四层板（0°/90°/90°/0°）的网格分布、模量比和边厚比对固有频率的影响。规则节点排布和非规则节点排布（$E_1/E_2=40$，网格＝21×21）的简支方形三层板（0°/90°/0°）的一阶频率和二阶频率的比较结果如图4和图5所示。规则节点排布和非规则节点排布（$E_1/E_2=40$，网格＝21×21）下的简支方形四层板（0°/90°/90°/0°）的一阶频率和二阶频率的比较结果如图6和图7所示。

表4　简支方形板（0°/90°/0°）的无量纲一阶固有频率（$E_1/E_2=40$）

Tab. 4　Non-dimensional fundamental frequency of the simply supported square laminated plate ($E_1/E_2=40$)

边厚比(a/h)	方法	$\bar{\omega}$
4	Ref.[26]	9.497
	Ref.[27]	9.322
	本文(21×21)	8.8921
10	Ref.[26]	15.270
	Ref.[27]	15.103
	本文(21×21)	14.7449
20	Ref.[26]	17.668
	Ref.[27]	17.641
	本文(21×21)	17.5014

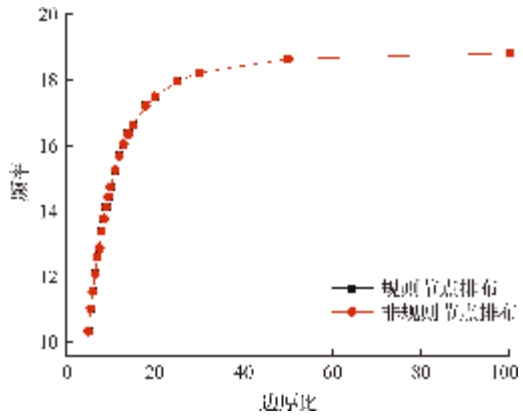

图4　规则节点排布和非规则节点排布（$E_1/E_2=40$，网格＝21×21）的简支方形板（0°/90°/0°）的一阶频率的比较

Fig. 4　Comparison of first-order frequency of the simply supported square plate (0°/90°/0°) by a regular grid pattern and an irregular grid pattern ($E_1/E_2=40$, grid=21×21)

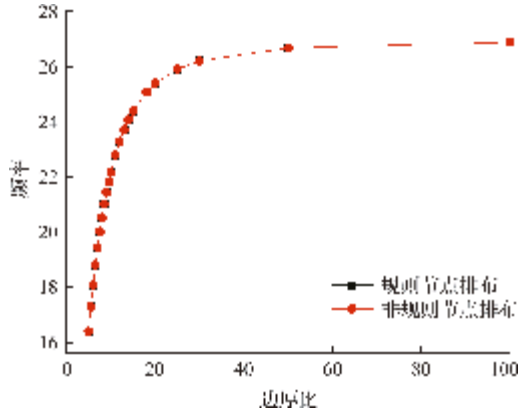

图5　规则节点排布和非规则节点排布（$E_1/E_2=40$，网格＝21×21）的简支方形板（0°/90°/0°）的二阶频率的比较

Fig. 5　Comparison of second-order frequency of the simply supported square plate (0°/90°/0°) by a regular grid pattern and an irregular grid pattern ($E_1/E_2=40$, grid=21×21)

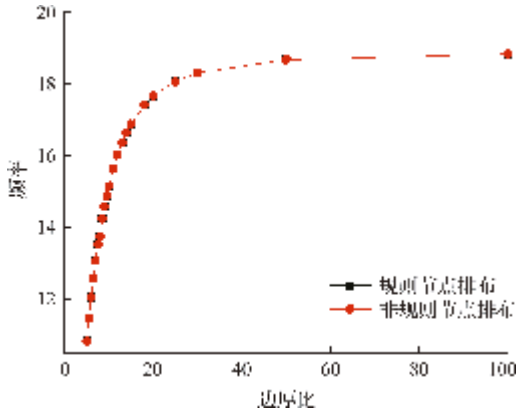

图 6 规则节点排布和非规则节点排布($E_1/E_2=40$,网格=21×21)对简支方形板(0°/90°/90°/0°)的一阶频率的比较

Fig. 6 Comparison of first-order frequency of the simply supported square plate (0°/90°/90°/0°) by a regular grid pattern and an irregular grid pattern ($E_1/E_2=40$, grid=21×21)

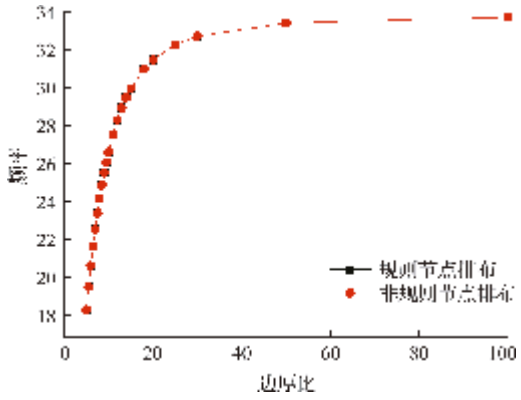

图 7 规则节点排布和非规则节点排布($E_1/E_2=40$,网格=21×21)对简支方形板(0°/90°/90°/0°)的二阶频率的比较

Fig. 7 Comparison of second-order frequency of the simply supported square plate (0°/90°/90°/0°) by a regular grid pattern and an irregular grid pattern ($E_1/E_2=40$, grid=21×21)

规则节点排布和非规则节点排布($a/h=10$,网格=21×21)下简支方形板(0°/90°/0°)的一阶频率和二阶频率的比较结果如图 8 和图 9 所示。从

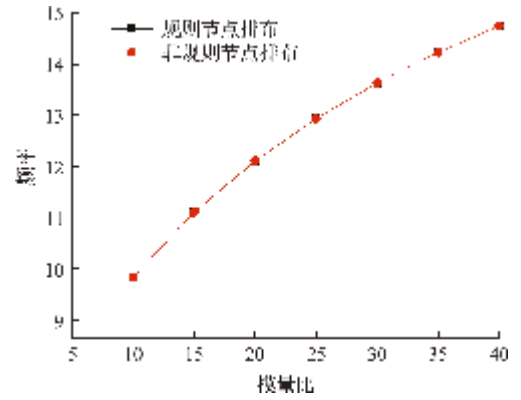

图 8 规则节点排布和非规则节点排布($a/h=10$,网格=21×21)下简支方形板(0°/90°/0°)的一阶频率的比较

Fig. 8 Comparison of first-order frequency of the simply supported square plate (0°/90°/0°) by a regular grid pattern and an irregular grid pattern ($a/h=10$, grid=21×21)

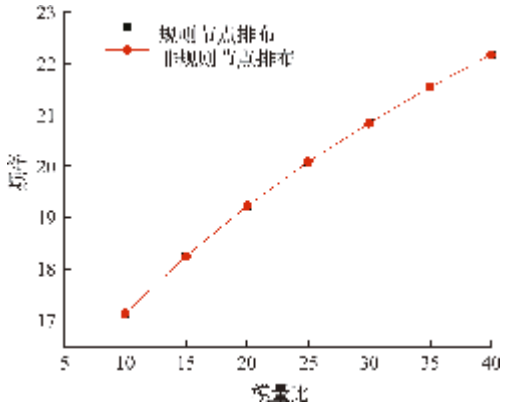

图 9 规则节点排布和非规则节点排布($a/h=10$,网格=21×21)下简支方形板(0°/90°/0°)的二阶频率的比较

Fig. 9 Comparison of second-order frequency of the simply supported square plate (0°/90°/0°) by a regular grid pattern and an irregular grid pattern ($a/h=10$, grid=21×21)

图 4～图 9 可以看出,如果网格点的数量足够大,则无量纲频率对网格分布不敏感。从图 4～图 7 可以看出,无量纲频率随着边厚比的增加而增加。从图 8 和图 9 可以看出,无量纲频率随着模量比的增加而增加。

5 结 论

基于层合梁的三角剪切变形理论,本文导出了角铺设复合材料层合板的微分控制方程。利用基于薄板样条径向基函数的无网格配置法离散的微分控制方程来预测对称叠层复合材料板的自由振动行为。通过数值实验,证明了用薄板样条径向基函数离散的三角剪切变形理论用于角铺设复合材料层合板自由振动分析的高精度和良好的收敛性。

参考文献(References):

[1] Rajapakse Y D S, Hui D. Marine composites and sandwich structures [J]. *Composites Part B: Engineering*, 2008, **39**(1): 1-4.

[2] Li M Z, Guedes Soares C, Yan R J. A novel shear deformation theory for static analysis of functionally graded plates [J]. *Composite Structures*, 2020, **250**: 112559.

[3] 项 松, 石 宏. 基于逆复合二次径向基函数的对称复合材料层合板自由振动分析[J]. 计算力学学报. 2011, **28**(1): 152-157. (XIANG Song, SHI Hong. Free vibration analysis of symmetric laminated composite plates based on the inverse multiquadric radial basis function [J]. *Chinese Journal of Computational Mechanics*, 2011, **28**(1): 152-157. (in Chinese))

[4] Kant T, Ravichandran R V, Pandya B N, et al. Finite

element transient dynamic analysis of isotropic and fibre reinforced composite plates using a higher-order theory[J]. *Composite Structures*, 1988, **9**(4): 319-342.

[5] Nelson R B, Lorch D R. A refined theory for laminated orthotropic plates[J]. *Journal of Applied Mechanics*, 1974, **41**(1): 177.

[6] Putcha N S, Reddy J N. Stability and natural vibration analysis of laminated plates by using a mixed element based on a refined plate theory[J]. *Journal of Sound and Vibration*, 1986, **104**(2): 285-300.

[7] Kant T, Pandya B N. A simple finite element formulation of a higher-order theory for unsymmetrically laminated composite plates[J]. *Composite Structures*, 1988, **9**(3): 215-246.

[8] Mantari J L, Guedes Soares C. Generalized hybrid quasi-3D shear deformation theory for the static analysis of advanced composite plates[J]. *Composite Structures*, 2012, **94**(8): 2561-2575.

[9] Mantari J L, Guedes Soares C. Optimized sinusoidal higher order shear deformation theory for the analysis of functionally graded plates and shells[J]. *Composites Part B: Engineering*, 2014, **56**: 126-136.

[10] Arya H, Shimpi R P, Naik N K. A zigzag model for laminated composite beams[J]. *Composite Structures*, 2002, **56**(1): 21-24.

[11] Ferreira A J M, Roque C M C, Jorge R M N. Analysis of composite plates by trigonometric shear deformation theory and multiquadrics[J]. *Computers & Structures*, 2005, **83**(27): 2225-2237.

[12] Wang S. Free vibration analysis of skew fibre-reinforced composite laminates based on first-order shear deformation plate theory[J]. *Computers & Structures*, 1997, **63**(3): 525-538.

[13] Khdeir A A, Reddy J N. Free vibrations of laminated composite plates using second-order shear deformation theory[J]. *Composite Structures*, 1999, **71**(6): 617-626.

[14] Khdeir A A, Librescu L. Analysis of symmetric cross-ply laminated elastic plates using a higher-order theory. Part II: Buckling and free vibration[J]. *Composite Structures*, 1988, **9**(4): 259-277.

[15] Akhras G, Li W. Static and free vibration analysis of composite plates using spline finite strips with higher-order shear deformation[J]. *Composites Part B: Engineering*, 2005, **36**(6-7): 496-503.

[16] Ferreira A J M, Roque C M C, Jorge R M N. Free vibration analysis of symmetric laminated composite plates by FSDT and radial basis functions[J]. *Computer Methods in Applied Mechanics and Engineering*, 2005, **194**(39-41): 4265-4278.

[17] Liew K M, Huang Y Q, Reddy J N. Vibration analysis of symmetrically laminated composite plates based on FSDT using the moving least squares differential quadrature method[J]. *Computer Methods in Applied Mechanics and Engineering*, 2003, **192**(19): 2203-2222.

[18] Atluri S N, Zhu T. A new Meshless Local Petrov-Galerkin (MLPG) approach in computational mechanics[J]. *Computational Mechanics*, 1998, **22**(2): 117-127.

[19] Belytschko T, Lu Y Y. Element-free Galerkin method[J]. *International Journal for Numerical Methods in Engineering*, 1994, **37**: 229-256.

[20] Liu G R. *Mesh Free Methods: Moving Beyond the Finite Element Method*[M]. New York: CRC Press, 2002.

[21] Kansa E J. Multiquadrics—A scattered data approximation scheme with applications to computational fluid-dynamics. I: Surface approximations and partial derivative estimates[J]. *Computer & Mathematics with Applications*, 1990, **19**(8-9): 127-145.

[22] Ferreira A J M, Batra R C, Roque C M C, et al. Static analysis of functionally graded plates using third-order shear deformation theory and a meshless method[J]. *Composite Structures*, 2005, **69**(4): 449-457.

[23] Ferreira A J M, Batra R C, Roque C M C, et al. Natural frequencies of functionally graded plates by a meshless method[J]. *Composite Structures*, 2006, **75**(1-4): 593-600.

[24] Reddy J N. *Mechanics of Laminated Composite Plates: Theory and Analysis*[M]. Boca Raton: CRC Press, 1997.

[25] Dai K Y, Liu G R, Lim K M, et al. A mesh-free method for static and free vibration analysis of shear deformable laminated composite plates[J]. *Journal of Sound and Vibration*, 2004, **269**(3-5): 633-652.

[26] Reddy J N, Phan N D. Stability and vibration of isotropic, orthotropic and laminated plates according to a higher-order shear deformation theory[J]. *Journal of Sound and Vibration*, 1985, **98**(2): 157-170.

[27] Akhras G, Li W. Static and free vibration analysis of composite plates using spline finite strips with higher-order shear deformation[J]. *Composites Part B: Engineering*, 2005, **36**(6-7): 496-503.

Free vibration analysis of laminated composite plates based on thin plate spline radial basis functions

SONG Wei-wei*[1,2,3], XIANG Song[1,2], ZHAO Rui[1,2], ZHAO Wei-ping[1,2], GUO Han[1,2]
(1. General Aviation Key Laboratory of Liaoning Province, Shenyang Aerospace University, Shenyang 110136, China;
2. Liaoning General Aviation Academy, Shenyang 110136, China;
3. Department of Civil Aviation, Shenyang Aerospace University, Shenyang 110136, China)

Abstract: Based on the trigonometric shear deformation theory of laminated composite plates, the governing differential equation of symmetric laminated composite plates is derived. The free vibration behavior of symmetric composite laminates is predicted using discrete governing differential equation derived from a meshless collocation method based on the spline radial basis functions for a thin plate. The natural frequencies of the laminated composite plates with different material parameters and geometric parameters were calculated and compared with some published results. The effects of the grid pattern modulus ratio, and the side-to-thickness ratio on natural frequencies are also studied. The results show that the calculation results of this article are in good agreement with the published results. The larger the number of nodes, the less sensitive the dimensionless frequency is to the grid distribution. The natural frequency increases with the increase of the edge thickness ratio and modulus ratio. Through numerical experiments, it is proved that the trigonometric shear deformation theory combined with the thin plate spline radial basis functions for a thin plate has high numerical accuracy and good convergence for the free vibration analysis of symmetric composite laminated plates.

Key words: trigonometric shear deformation theory; laminated composite plate; free vibration; thin plate spline radial basis function; natural frequency

(上接第 934 页)

LBM simulation of the effect of salinity on dissociation characteristics of methane hydrate

GENG Fei-fan[1], DONG Bo*[1], ZHOU Xun[2], ZHANG Ya-jin[1], CUI Jia[1], LI Wei-zhong[1]
(1. Key Laboratory of Marine Energy Utilization and Energy Conservation of the Ministry of Education, School of Energy and Power Engineering, Dalian University of Technology, Dalian 116024, China;
2. School of Vehicle and Transport Engineering, Henan University of Science and Technology, Luoyang 471003, China)

Abstract: The dissociation process of marine methane hydrate is affected by seawater salinity. Based on the lattice Boltzmann method, a numerical model is established to simulate the dissociation of methane hydrate in brine at the pore scale. The dissociation kinetics of methane hydrate, mass transfer of methane and salt, gas-liquid two-phase flow and heat transfer are comprehensively considered, and the effect of salinity on methane hydrate dissociation is described by introducing additional source terms. On this basis, this paper analyzes the effect of salinity on dissociation characteristics and heat transfer characteristics of methane hydrate. The results show that the dissociation rate of methane hydrate in the salt solution is significantly faster than that in pure water. The dissociation rate increases with salinity and the dissociation duration decreases with salinity. Besides, the average temperature in the calculation domain drops sharply at the initial stage of hydrate dissociation and gradually increases to the initial inlet temperature. The lowest average temperature increases with salinity. Therefore, the increase in salinity can accelerate the dissociation rate of methane hydrate and reduce the heat absorption of hydrate dissociation.

Key words: methane hydrate; salinity; lattice Boltzmann method; dissociation characteristic; heat transfer characteristic